Investigations on hydrogen-assisted cold cracking of laser welded AHSS

Anton Sampiero Hopf (✉ anton_sampiero.hopf@mercedes-benz.com)

Mercedes-Benz Group AG   https://orcid.org/0000-0001-8673-6091

Sven Jüttner

Otto-von-Guericke-University Magdeburg: Otto-von-Guericke-Universitat Magdeburg

Klaus Goth

Mercedes-Benz Group AG

Michael Luttmer

Mercedes-Benz Group AG

Abstract

This study aims to investigate the impact of various surface conditions prior to welding on the susceptibility of materials to cold cracking, including an analysis of fracture surfaces. Additionally, a novel method is introduced for quantifying the presence of diffusible hydrogen using thermal desorption mass spectroscopy (TDMS). This method allows for the determination of diffusible hydrogen concentration in thin sheet welded joints without use of welding consumables. Three different cold-rolled Advanced High-Strength Steel (AHSS) samples with different surface conditions, such as coatings, lubrication, or water, are examined to assess their susceptibility to cold cracking. In addition to measuring the diffusible hydrogen content in both the base material and the coating, the overall hydrogen content of the base material is also measured using the melt extraction (ME) method. The new method for quantifying diffusible hydrogen in weld metal is applied to investigate different welding variations, intentionally introducing hydrogen through coatings and hydrogenous fluids on the sheet surface. By combining the assessment of cracking susceptibility and hydrogen content, a better understanding of critical hydrogen levels leading to hydrogen-assisted cracking (HAC) is achieved. The results of this study demonstrate that the occurrence of cold cracking in specific AHSS samples increases when either lubrication or both coating and water or lubricant are added. Additionally, the presence of diffusible hydrogen in the welds of all materials is found to increase with the introduction of hydrogenous layers to the material. Although a critical hydrogen content is identified, no clear correlation between the amount of hydrogen and cracking susceptibility can be determined. These findings have significant implications for the welding of cold-formed AHSS, particularly in the automotive industry where safety and lightweight design are of paramount importance.

1 Introduction

The lightweight concept in automotive industry requires the development of new steel concepts to achieve their diverse and sometimes contradicting objectives. Advanced high strength steels (AHSS) are particularly promising due to their high strength and good formability, which result in significant weight reductions and increased passenger safety in accidents. [1] In addition to the development of AHSS sheets for automotive components, the use of laser welding has become increasingly popular in automobile production due to its numerous benefits. Compared to conventional thermal joining methods, laser welding provides beside one-sided accessibility of joining parts, a narrow and deep penetration depth, resulting in a high aspect ratio of the welded joint and minimal heat input into the material leading to reduced processing times. [2]

The use of AHSS presents the risk of hydrogen embrittlement, leading to material degradation and reduced mechanical properties. [3–5] Hydrogen can enter the material through various production and processing steps and accumulate due to stresses and plastic deformation. Laser welded joints of AHSS are particularly susceptible to hydrogen-assisted cracking (HAC), caused by:

- susceptible high strength microstructure to HAC,

- tensile stresses imposed during welding,
- and high levels of diffusible hydrogen.

Both the weld metal and heat affected zone can be affected by HAC, with the latter being more prevalent due to the combination of microstructure and tensile restraint. [6] High strength steels increase the risk of hydrogen embrittlement due to their lower solid solubility of hydrogen. Several studies have been conducted evaluating the influences of body-in-white environment on the hydrogen intake in AHSS welded joints. [7–11]

Hydrogen can be generated from multiple sources during the fabrication of welds, with electrochemical reactions and the dissociation of molecular hydrogen into atomic hydrogen at high temperatures being the primary mechanisms [12]. These processes contribute to the presence of hydrogen in the welds. In a broader classification, the sources of hydrogen during weld fabrication can be divided into two main categories based on their causes: those originating from the fabrication process itself, which include trapping or coating-related factors, and those occurring during welding, such as the presence of moisture in the atmosphere or hydrogenous layers on the material surface [13–18].

To accurately evaluate hydrogen embrittlement risk and understand the phenomenon, it is important to quantify the influence of hydrogen in critical areas, which can be challenging due to the small size of hydrogen atoms and their tendency to escape from materials. Modern evaluation procedures are necessary to predict the risk of hydrogen-induced time-delayed failure, involving hydrogen source, uptake, diffusion, and damage kinetics.

2 Measurement of hydrogen content

Various methods can be employed to determine the hydrogen content in metals, including assessments conducted before, during, or after the manufacturing process, as well as during service conditions. However, given the potential degradation of mechanical properties associated with HAC, highly analytical techniques are necessary. One commonly used method for measuring hydrogen and quantifying diffusible and trapped hydrogen concentrations in metals is thermal desorption spectroscopy (TDS).

The TDS technique utilizes a solid or melt extraction approach and can be applied to both solid and molten samples. Nitrogen gas with a purity of 99.999% is employed as the carrier gas, as it exhibits a substantial difference in thermal conductivity compared to hydrogen. To achieve high-resolution measurements of hydrogen in conjunction with the TDS technique, different detection systems have been developed, such as thermal conductivity devices (TCD) and mass spectrometers (MS) [19].

Calibration for these detector units can be performed using gas calibration or certified reference materials. However, certified reference materials for diffusible hydrogen are not readily available due to its high mobility, even at room temperature. TDS experiments can be conducted using isothermal or thermal procedures, utilizing a controlled furnace to heat the sample.

2.1 Diffusible hydrogen in welds

In Europe, the standard DIN EN ISO 3690:2018-12 [20] is utilized for the measurement of diffusible hydrogen in arc-welded metal. This standard is comparable to the American AWS A4.3-93 [21] and the Japanese JIS Z 3113 [22] standards, although there may be slight variations in the specified methods. Generally, these standards are largely equivalent. For the purposes of this study, DIN EN ISO 3690 [20] is adopted as the benchmark standard, with minor modifications made to adapt it for use of hydrogen quantification of laser-welded samples without additional welding consumables.

Numerous investigations have been carried out to study the behavior of hydrogen in advanced and ultra-high strength steels. These studies have contributed to the evaluation of critical loading scenarios in mechanically stressed components. [23–26] It has been observed that plastic deformation affects the mobility and storage of hydrogen, resulting in a reduction in diffusivity. [27] This phenomenon is attributed to the creation of trapping sites such as dislocations, distortion fields, and micro-cracks, which exert varying effects on diffusion processes depending on their nature.

Determining the hydrogen content in weld and deposited metal can be reliably accomplished using established procedures. However, measuring the local hydrogen concentration poses challenges due to the high mobility of hydrogen atoms within a crystalline lattice. Consequently, calculation methods are commonly employed to assess hydrogen diffusion, and physical-mathematical models have been developed for this purpose. [28, 29] These models necessitate the use of numerical methods and suffer from the limitation that their results are often difficult to generalize.

2.2 New method for determination of diffusible hydrogen concentration in laser-welded seams

To address these challenges, an approximate analytical model for hydrogen diffusion was developed in this study. The model takes weld and joint dimensions, different initial hydrogen concentrations in the weld metal and base metal into account. The model was demonstrated using different surface conditions before welding and the diffusible hydrogen contents were compared to the cold cracking susceptibility of the different samples.

In accordance with DIN EN ISO 3690 [20], a table of temperature/time combinations suitable for diffusible hydrogen analysis is provided. These combinations are designed to guarantee complete diffusion of all diffusible hydrogen from the sample. Contrary for the aim of this study the time for diffusion between welding and measurement has to be minimized.

Procedure for sample preparation.

In order to determine the diffusible hydrogen concentration in laser welded joints, cold cracking test samples with two weld seams, dimension of 45 × 105 × 1.5 mm³ and either fully overlapped or welded as bead on plate according to Hopf et al. can be used. [30]

Proper handling of specimens is crucial between welding and hydrogen measurement because of hydrogen's high atomic-level mobility, particularly at elevated temperatures, owing to its small size. This has been emphasized in [31–33]. Figure 1, closely linked to DIN EN ISO 3690 [20], illustrates the appropriate handling of welded samples before the start of measurement.

It is crucial that samples be immediately cooled below − 190°C to ensure the least possible hydrogen diffusion. [20, 34] The separation process of the lower and upper sheet is absolutely necessary to completely remove zinc, oil, or any other residues that could distort the hydrogen signal before the measurement. All steps until thawing should consider keeping the samples frozen, and in case of longer handling, they should be intercooled. While uncoating, inhibited hydrochloric acid should be used for the preservation of hydrogen uptake. [27]

Normalization of the measured hydrogen concentration

The two ways of normalization for diffusible hydrogen contents proposed by DIN EN ISO 3690 [20], shown in Fig. 2, are:

- H_D: The diffusible hydrogen content is calculated by dividing the effused volume of hydrogen by the weight difference of the specimen before and after welding, and then multiplying by 100. The referenced mass is the deposited weld metal, and thus the unit of H_D is mL/100 g of weld metal. (Fig. 3, left)
- H_F: The diffusible hydrogen content is calculated by dividing the effused volume of hydrogen by the total mass of the molten material (base metal and deposited weld metal). The penetration depth of the weldment must be known, which requires evaluating etched micrographs of every sample, ideally from both sides to see changes in the penetration profile. The unit of H_F is ppm (with respect to the mass of the molten material). (Fig. 3, middle)

Klett et al. showed that both methods are used to compare the diffusible hydrogen content of different welding procedures or materials. The choice of method depends on the information available and the purpose of the analysis. H_D is simpler and easier to use, but it only considers the deposited weld metal. H_F takes both the base metal and the deposited weld metal into account but requires more information and analysis. [35]

It is important to highlight that in bead-on-plate/overlap laser welding, no material is added and solely the base metal is liquefied. (Fig. 2, right).

The quantification of hydrogen concentration using the TDS measurement method provides an average value that represents the entire sample. However, in order to determine the diffusible hydrogen concentration specifically in the heat-affected region, it is essential to differentiate between various areas including the base metal, weld metal, and the overall hydrogen concentration of the welded sample. In the case of laser welding without filler material, the hydrogen content in the heat-affected area can be calculated using the following equations:

$$V_{tot} = V_w + V_{bm} \ (1)$$

This equation separates the whole sample volume V_{tot} into two volumes. V_w the welded volume of the sample and the base material V_{bm}, assuming that the narrow HAZ of the weld seam mostly remained not molten and is taken into account as base material.

$$V_{tot} \cdot h_{tot,300°C} = V_w \cdot h_{w,300°C} + V_{bm} \cdot h_{bm,300°C} \ (2)$$

The second equation weights the diffusible hydrogen contents of both the base metal and the overall welded sample. Since volumes of the entire sample as well as weld pool and hydrogen contents except for the hydrogen content of the weld metal $h_{w,300°C}$ are already known, the missing value can be calculated.

$$h_{w,300°C} = V_{tot} / V_{weld} \cdot (h_{tot,300°C} - h_{bm,300°C}) + h_{bm,300°C} \ (3)$$

By utilizing the suggested testing method and considering the findings from investigations on cold cracking, it becomes possible to identify potential effects regarding the impact of hydrogen build-up in welded materials and the resulting occurrence of cracks.

3 Experimental procedure

3.1 Material characterization

For the investigation three hot-dip galvanized GI50/50 coated AHSS steels, CR700Y980T-DH, CR700Y980T-DP, CR780Y980T-CH with an ultimate tensile strength level of 1000 MPa and a thickness of 1.52 ± 0.1 mm were systematically studied in the present work. The chemical composition and calculated carbon equivalent of the steels are shown in Table 1.

Table 1
Chemical composition of steels DH, CH and DP in wt.%

	C	Si	Mn	Al	Cr + Mo	Ti	Nb	Cu	Ni	CEQ[1]
DH	0.150	0.94	2.47	0.22	0.12	0.005	0.001	0.037	0.04	0.57
DP	0.083	0.47	2.27	0.04	0.52	0.028	0.033	0.017	0.03	0.39
CH	0.087	0.46	2.32	0.04	0.52	0.028	0.023	0.015	0.04	0.40

Additionally Table 2 displays the results from quasi-static tensile tests according to DIN EN ISO 6892-1 that were performed on a universal testing machine to determine the mechanical properties of the investigated material [11].

Table 2
Mechanical properties of steels DH, CH and DP

Steel	$R_{p0,2}$ [MPa]	R_m [MPa]	A_g [%]	A_{80} [%]
DH	838	1034	8.2	12.5
CH	880	1032	7.0	11.0
DP	712	1040	7.2	10.7

The microstructure was investigated using a light optical microscope (LOM) and a scanning electron microscope (SEM). For microstructural investigations the materials were grinded, polished and etched with 3% Nital for 5 s.

3.2 Cold cracking test and welding parameters

For evaluating the susceptibility to cold cracking the testing method according to Hopf et al. was used for different surface conditions of the same material. [30] All samples were welded with 0.1 mm dimples for the zinc degassing gap between upper and lower sheet.

Figure 3 displays the sample dimensions used for cracking susceptibility evaluation.

For welding of the samples a Yb:YAG disc laser with a maximum power of 8 kW (Trumpf, TruDisk8001) and a programmable focusing optic (Trumpf, 3D PFO) was used both for dimpling and welding. All materials were welded with the same welding parameters displayed in Table 3. The corresponding heat input E is calculated with the following equation:

$E = P/v$ (4)

with P for laser power and v for welding speed, respectively.

Table 3
List of welding parameters

Power [W]	Welding speed [mm/s]	Heat input [J/mm]
5600	75	75

The focal spot was 0.6 mm in diameter. The laser beam was used adjusted laterally and compressed air pressed through the crossjet nozzle protected the safety glass of the optics from pollution during

welding. The samples were welded without shielding gas. For clamping the proposed device from SEP 1220-3 was used with pneumatically controlled copper clamps. [37]

Aim of the cold cracking investigation was to evaluate the materials susceptibility for delayed cracking under different conditions. For each material the coated and uncoated state was investigated. The steels were uncoated with 18.5% hydrochloric acid inhibited with 3.5 g/l hexamethylenetetramine. Each variation was welded in cleaned and lubricated condition. The samples were cleaned using acetone and lubricated with 3 g/m² of forming oil (Multidraw, Fa. Fuchs).

A detailed overview of the investigated surface variations is given in Table 4.

Table 4
List of variations for cold crack testing

Variation		Index
Coated	Cleaned	Cleaned
	Cleaned + Lubricated	Lubricant
	Cleaned + Wetted	Water
Uncoated	Cleaned	Uncoated
	Cleaned + Lubricated	Unc. + Lub.

3.3 Hydrogen measurement in AHSS and laser-welded joints

For the analysis, a hydrogen analyzer Galileo G8 (Bruker AXS GmbH) equipped with a quadrupole mass spectrometer based on the thermal desorption spectroscopy (TDS) method was utilized. The measurement system follows the carrier gas approach, which enables the extraction of molten material and artificial aging. High-purity nitrogen gas (N2 5.0) serves as the carrier gas for hydrogen analysis. To determine the diffusible hydrogen, artificial aging is employed, whereby samples can be heated in an infrared furnace with a maximum temperature of 900°C. The heating process can be controlled using either isothermal temperature regimes or temperature ramps, where the temperature increases gradually over time. A thermocouple is placed on the sample to monitor the set heating rate and record the temperature. Before measuring gas-calibration of the system is performed. The hydrogen content of investigated samples are then evaluated by integrating the signal curves $Signal$ and division of calibration factor K multiplied with the sample weight w_i according the following equation

$$h_i = Signal / (K \cdot w_i) \quad (5)$$

In the present study, artificial aging is carried out at an isothermal temperature of 300°C with a system-controlled maximum heating rate to eliminate potential effects of different heating rates among the samples. The determination of the total hydrogen content is conducted through melt extraction (ME) using the same instrument at a temperature of 1800°C.

Table 4 provides an overview of all the investigated variations.

Table 4
List of variations for measurements of hydrogen content

Variation		Measuring Method	Temperature
Coated	Base Material	TDS	300 °C
	Cleaned	TDS	300 °C
	Cleaned + Lubricant	TDS	300 °C
	Cleaned + Wetted	TDS	300 °C
Uncoated	Base Material	ME	1800°C
	Base Material	TDS	300 °C
	Cleaned + Argon	TDS	300 °C
	Cleaned	TDS	300 °C
	Cleaned + Lubricant	TDS	300 °C

The experimental setup involves a systematic exploration of various factors affecting hydrogen content. The investigation begins by examining the diffusible hydrogen originating from the material itself during shielded welding (Argon, 15 l/min) of uncoated material. Subsequently, the influence of the welding environment is examined by conducting welding without shielding gas, still using uncoated material. The study then progresses to investigate the impact of a coating layer or the addition of an extra lubricant. Furthermore, the study explores potential interactions resulting from the welding of combinations of coated and lubricated or wetted surfaces. In this regard, a layer of 3 g/m² of lubricant is applied prior to welding, or water is dispersed beforehand. The use of water also simulates the presence of condensed water in different climate conditions during the welding process, and it helps eliminate unknown factors associated with the interaction of oil and the laser beam.

4 Results

4.1 Materials

Microstructure of base material

All three steels exhibit distinct differences in grain orientation and grain size. DH1000, characterized as a nonconventional quenched and partitioning (Q&P) dual-phase steel, has an average grain size of 3.571 µm. It displays a high ratio of light grains, which aligns well with the presence of tempered martensite/martensite that appears lighter after etching. Small areas of dark regions correspond to ferrite, and there are also small amounts of retained austenite, contributing to higher formability, adjusted through quenching and partitioning process.

The conventional dual-phase steel DP1000, possesses the smallest average grain size of 1.590 µm. It features a predominantly ferritic matrix with uniformly dispersed martensite and a prominent grain orientation. The complex phase steel CH1000, also chemically identical but differently processed, exhibits a slightly larger average grain size of 2.230 µm. Its microstructure comprises granular bainite, dispersed martensite, and (recovered) ferrite, similar to DH1000, with minimal portions of retained austenite. These characteristics result from the complex processing cycle including intercritical annealing treatment employed for this steel.

Differences in microstructure of the steels are illustrated in Fig. 5.

Microstructure and hardness of welded materials.

After welding with equal heat input all three materials show almost identical parallel weld pool shape. Hardness values for different surface variations of the same material show no differences. Due to the high cooling rates and associated solidification dynamics, a fine visible solidification line can be observed at the center of all weld seams, which is formed by the convergence of the solidification fronts during cooling.

For each material one hardness profile and cross-section is displayed in Fig. 6.

Base material hardness of DP1000 and DH1000 is 370 HV0.1 which is 20 HV0.1 higher than CH1000 at 351 HV0.1. In the fusion zone DP1000 and CH1000 show same hardness of 449 HV0.1, while hardness of DH1000 reaches 473 HV0.1. The displayed cross-sections in combination with the hardness value show the hardening and formation of martensitic weld material. The higher hardness values in the weld bead DH1000 correlates with the materials higher carbon content and validates the higher calculated carbon equivalent. CH1000 and DP1000 reach a hardness peak at 480 HV0.1 and DH1000 at 503 HV0.1. Overall the hardness delta from base material to weld is 100 HV0.1 for DH1000 and CH1000, while DP1000 is 70 HV0.1. Regarding the delta from maximum to minimum value in the HAZ DH1000 is 173 HV0.1, CH1000 150 HV0.1 and DP1000 142 HV0.1.

4.2 Cold cracking susceptibility

According to Hopf et al. [30] the inspection interval of the welded samples was performed after welding, after 1 h, after 1 day and after 1 week. Final results for the susceptibility are calculated with the following equation:

Cold cracking susceptibility = number of cracked seams after 7 days / total amount of weld seams (6)

Figure 7 shows increase in counted cracks over time after welding for different surface conditions of all three steels.

None of the welded variations of DP1000 exhibited delayed cracking after 7 days. The same result was observed when comparing the uncoated and coated variations for DH1000 and CH1000. However, delayed cracking was observed for both steels when lubricant was applied on uncoated and coated material as well as for the variations with water on the coated surface.

For DH1000, immediately after welding, no cracks were detected in the uncoated and lubricated condition. However, after 1 hour, 7 out of 20 welds exhibited cracks, and no further cracking was observed after 7 days. The coated surface with additional lubricant or water showed cracks right after welding, with 4 out of 20 and 10 out of 20 welds, respectively. Inspection after 1 hour revealed an increase in cold cracks to 40% for the water variation and 70% for the lubricant on the coated surface. However, both variations did not display further cracking by the end of the 7-day inspection period.

Material CH1000 showed cracks right after welding in the uncoated and lubricated variation, as well as in both coated variations with lubrication and water. Both coated variations exhibited cracks in 4 out of 20 welds for water on the surface and 7 out of 20 welds for lubrication. After one hour, both variations reached their final amount of cracks, with 60% for water and 75% for lubrication. The uncoated and lubricated variation exhibited 35% cracking after 1 hour and reached the final amount of 8 cracked welds after 24 hours. No difference was observed after the last inspection conducted 7 days after welding.

4.3 Fractography

The analysis of brittle crack morphology and the examination of delayed cracking patterns provide further validation of previous research findings. [38, 30] Notably, a distinct solidification crack, resulting from rapid cooling rates, is observed originating from the end crater. Subsequently, the crack propagates outward from the crater, extending in the opposite direction of the welding process. It predominantly follows the central region of the weld seam and terminates in close proximity to the starting point of the weld seam.

To visually illustrate this phenomenon, Fig. 8 presents a cross-sectional view showcasing a cold crack situated in the middle and on the top and bottom surfaces of a fractured CH1000 weld, with the end crater positioned on the left side.

For further examination and analysis of the patterns and features of fractured surfaces related to the delayed cracking behavior of the steels, a cracked sample of DH1000 is subjected to SEM analysis. As shown in Fig. 8 the cold crack propagate mainly along the weld seam center halving the weld and indicating a favored crack propagation along the solidification line.

As previously described, the origin of cold cracking can be traced back to the solidification crack in the end crater. By focusing on the bottom of the end crater b), two distinct areas can be observed. The first area consists of solidification or hot cracks c) characterized by a dendritic structure, while the second area corresponds to cold cracks d) exhibiting transgranular and intergranular fracture surfaces. These observations provide clear indications of HAC, as previously demonstrated by [39, 40].

4.4 Characterization of hydrogen contents

Before examining the impact of welding on hydrogen uptake or loss, the total and diffusible hydrogen contents of the base materials were analyzed using ME at 1800°C and TDS at 300°C. For DH1000, the total hydrogen amount is 0.84 ppm, and the diffusible amount in the uncoated base material is 0.02 ppm. Both CH1000 and DP1000 steels have a total hydrogen amount of 1.87 ppm and 1.80 ppm, respectively. Similar to DH1000, both steels contain 0.03 ppm and 0.04 ppm of diffusible hydrogen in an uncoated state. The coating influence for DH1000 is 0.28 ppm, while the diffusible hydrogen level for CH1000 and DP1000 is at 0.08 ppm and 0.07 ppm, respectively.

Figure 10 displays the hydrogen contents of the base material, including diffusible and total proportions, as well as the diffusible content in the coated state.

After following the process steps described in section 2.2 the hydrogen contents from welds with different surface conditions are normalized to the local weld seam contents. The qualitative behavior of the measurement signals is similar for all materials and surface conditions, which is why only one example will be discussed. The TDS signal remains nearly unchanged, corresponding to 0.02 ppm hydrogen in the uncoated base material. However, variations in the surface condition result in an increase in both the height and width of the signal. Each signal curve reaches its peak between 200°C and 250°C, and then decreases to its initial level at the final measurement temperature of 300°C. The peak of the signals progressively rises, while the curve broadens with alterations in the surface condition.

Diffusible hydrogen contents for different surface conditions

With results of diffusible hydrogen contents in the base materials, as discussed in section 2.2 for normalization of the hydrogen content in laser welds the hydrogen contents for the weld seam can be calculated with formula (3). The average weld pool volume used for calculation was 77.56 mm³ compared to a total sample volume of approximately 402.24 mm³.

Figure 11 displays exemplary for the obtained hydrogen content from the measurement and the corresponding weld seam contents for coated welds of each material and weld pool area in longitudinal and transversal direction.

All further results are considering the hydrogen contents in the weld metal. For DH1000 different signals with corresponding peaks from TDS measurement of welded samples as well as resulting hydrogen content in the weld are displayed in Fig. 12.

When welding uncoated material with argon as the shielding gas, there is an initial increase to 0.75 ppm of diffusible hydrogen. Subsequently, the welding process without shielding gas further elevates the diffusible hydrogen level to 1.29 ppm. Comparing the effects of coating and lubrication both exhibit similar outcomes. The presence of zinc leads to 1.43 ppm hydrogen in the weld, while lubrication results in 1.51 ppm. Applying lubrication to the surfaces of coated material raises the measured hydrogen content to 2.09 ppm. In the presence of water on the sample surfaces, the hydrogen increase reaches up to 2.78 ppm.

Based on the obtained results for DH1000, laser welding, when shielded with argon, facilitates the release and transfer of trapped hydrogen to diffusible hydrogen, unaffected by the surrounding atmosphere. However, in the absence of shielding, welding without protection allows the uptake of more than 0.50 ppm hydrogen from atmospheric humidity. Introducing a hydrogen-containing layer such as zinc coating or lubrication onto the uncoated base material further amplifies the measured diffusible hydrogen content in the weld seam, increasing it by approximately 0.14 ppm and 0.22 ppm, respectively. The addition of a lubricant or water on the coated steel surface leads to a significantly higher increase in hydrogen content. Combining zinc with forming oil enhances the hydrogen content by approximately 0.8 ppm compared to uncoated welds. Notably, welding coated material with a layer of condensed water elevates the hydrogen content in the weld by 1.69 ppm.

Regarding the chemically almost identical steels CH1000 and DP1000, both materials exhibit less than 0.04 ppm hydrogen in their base material, as mentioned earlier. A change in surface conditions for both materials results in a similar stepwise increase in the hydrogen content of the weld seam, qualitatively comparable to DH1000. Shielded welding of uncoated CH1000 raises the measured hydrogen content to 0.58 ppm, while for DP1000, the hydrogen level rises to 0.75 ppm. When uncoated CH1000 is welded without argon, the influence of atmospheric hydrogen leads to a hydrogen level of 0.84 ppm. In contrast, DP1000 shows no significant further hydrogen uptake without shielding gas. The impact of zinc, with a hydrogen level of 1.14 ppm, is 0.33 ppm lower than that of lubricated uncoated CH1000. In contrast to DP1000, both surface changes result in an equal increase in hydrogen content, approximately 1.42 ppm and 1.45 ppm, respectively. Notably, a significant difference arises between the two materials when welding lubricated and coated samples. For CH1000, the hydrogen content increases significantly, akin to DH1000, reaching 2.60 ppm, while DP1000 maintains a relatively stable hydrogen level of approximately 1.61 ppm. The substitution of lubricant with water on the coated surface slightly enhances the diffusible content of CH1000 to 3.25 ppm, whereas for DP1000, the reaction to wetted surfaces yields a hydrogen level of 3.55 ppm.

The hydrogen contents for CH1000 and DP1000 are displayed in Fig. 13.

When comparing the hydrogen absorption behavior of both materials, it is observed that shielding DP1000 during welding results in a similar hydrogen content of approximately 0.75 ppm in the weld compared to welding without argon. This indicates a high solubility of trapped hydrogen in DP1000 during the welding process. In contrast, CH1000 releases over 0.5 ppm of hydrogen through the release of

trapped hydrogen and gains an additional 0.25 ppm of diffusible hydrogen from the atmosphere when welded without shielding. Similar to DH1000, the addition of zinc or lubricant layers to CH1000 increases the hydrogen content by 0.3 ppm and 0.6 ppm respectively, with lubricant having twice the influence compared to zinc coating. Once again, a disproportional increase in hydrogen content is observed when investigating coated and lubricated CH1000. For DP1000, the addition of coating, lubricant, or both simultaneously results in a hydrogen uptake of approximately 0.8 ppm compared to uncoated welds. The application of water on the coated surface leads to a disproportionate increase in the diffusible hydrogen content in the weld for both materials. In CH1000, the diffusible hydrogen content slightly increases by 0.6 ppm compared to lubricant, while in DP1000, it increases by over 2 ppm.

5 Discussion

The base materials used in this study exhibited different microstructures before welding. DP1000 primarily consisted of martensite and ferrite, with a lower yield strength compared to DH1000 and CH1000. The latter two materials had higher yield strength levels and contained retained austenite in their microstructure, which contributed to increased ductility upon loading. [41, 42] The grain sizes varied, ranging from 1.59 µm for DP1000 to 2.23 µm for CH1000 and 3.57 µm for DH1000. This led to larger grain boundary areas, resulting in a decrease in trapped hydrogen content from 1.87 ppm for DP1000 to 1.80 ppm for CH1000 and 0.87 ppm for DH1000. These findings align with previous studies that have shown the effect of decreasing grain size on increasing grain boundary areas and increasing hydrogen traps. [43, 44] Further investigations on the diffusion and trapping behavior of the materials are recommended to gain a better understanding of hydrogen uptake during welding under different surface conditions.

The susceptibility to cold cracking varied among the materials based on the pre-welding surface condition. DP1000 exhibited no cold cracking, whereas both DH1000 and CH1000 experienced cracking when uncoated material was additionally lubricated or when an additional hydrogen-containing layer of lubricant or water was applied to the coated steel. The presence of time-delayed cracking and the observation of brittle fracture surfaces displaying transgranular and intergranular characteristics provided clear evidence of HAC. This aligns with prior studies. [45–47] The occurrence of cold cracking originating from the solidification crack in the end crater, which can be regarded as a welding defect or geometric notch, supports the occurrence of cold cracking [16, 48].

For both materials with cracks the coated and additionally lubricated condition was most severe. Maeda et al. presented an investigation method utilizing x-ray for crack detection with cracks occurring within less than 1 minute after welding [38]. Visual inspection, as recommended by Hopf et al. [30], proved to be a reasonable method for crack investigation, as no further cracks were observed after 24 hours. Therefore, the crack investigation after 7 days can be shortened as it seems redundant.

The analysis of diffusible hydrogen content in the base materials revealed negligible amounts of diffusible hydrogen in the investigated AHSS. The measured levels were below 0.03 ppm, confirming

previous studies indicating the minimal presence of diffusible hydrogen in this type of steel. [49–51] The low diffusible hydrogen contents in CH1000 and DP1000 can be attributed to their common hot-dip galvanization process. However, DH1000 exhibited a higher hydrogen content in the coating or the area between the steel and coating, likely due to differences in the coating facility. The phenomenon of hydrogen effusion from the coating has been observed in previous studies. [27, 24] Crucial for the normalization of the hydrogen content is an adequate ratio of base material to weld metal. In this study the ratio averaged approximately 1 to 5 which effectively combined goals of low heat input while sample preparation and reduced impact of low level hydrogen from the base material. Regarding the preparation steps, the sample cutting could be changed to punching or another more precise and repeatable process. Nevertheless the results show high reproducibility. Lower hydrogen contents of the uncoated material compared to the coated state also approves the uncoating method with acid since no hydrogen uptake took place. It should be mentioned that this effect is dependent on processing times which should be kept minimal which contributes to Backhaus. [27]

The hydrogen content in all steels increases when hydrogen-contributing factors are introduced before the welding process. These findings align with the existing model for hydrogen uptake during gas metal arc welding processes. [52, 53] Both cracking-prone steels, DH1000 and CH1000, exhibit similar responses to different surface conditions, while DP1000 primarily releases hydrogen during welding and shows less sensitivity to external hydrogen sources such as zinc coating or lubrication. However, when water is added to its coated surface, DP1000 demonstrates a similar non-proportional effect as DH1000 and CH1000 with hydrogen-containing layers.

The diffusible weld hydrogen contents and its evaluated cold cracking susceptibility of different surface conditions are displayed in Fig. 14.

A comparison of diffusible hydrogen in welds under different surface conditions reveals a critical hydrogen content for cracking. However, no correlation is observed between increasing hydrogen content and increasing cracking susceptibility. This can be explained by the fact that the method used in this study considers the overall hydrogen content in the weld, which may not accurately reflect the hydrogen distribution in the critical area where hydrogen accumulation is necessary for crack propagation, as proposed by the hydrogen enhanced localized plasticity theory. [54–56] To gain further insights into the material-dependent cracking susceptibility, future studies should focus on investigating the diffusion characteristics of the materials and specifically the weld materials.

6 Conclusion

The current investigation aimed to assess the impact of surface conditions prior to laser welding on cold cracking in AHSS using a self-restraint cold cracking test method. The hydrogen content of three different AHSS samples was also analyzed using TDS and ME techniques. Additionally, a method for quantifying the diffusible hydrogen content in welding without consumables was introduced.

The following findings were obtained from this study:

- Steels DP1000 and CH1000, which have similar chemical compositions but different processing methods leading to distinct microstructures, exhibited the same amount of trapped hydrogen, approximately 1.80 ppm. The DH1000 material contained less than half of this amount.
- All three steels contain diffusible hydrogen below 0.05 ppm. The hydrogen contribution from the coating was also below 0.05 ppm for CH1000 and DP1000, whereas DH1000 exhibited a diffusible hydrogen content of 0.3 ppm originating from the coating.
- DP1000 exhibited no susceptibility to cold cracking, while DH1000 and CH1000 experienced cracking when additional hydrogen-containing liquids were applied to both uncoated and coated surfaces. The critical hydrogen content for cold cracking is reached 1.47 ppm for CH1000 and 1.51 mm for DH1000.
- During the welding process, trapped hydrogen was released from the base material, ranging from 0.5 ppm to 0.75 ppm. Shielding with argon gas during welding reduced the hydrogen uptake by 0.5 ppm for DH1000 and by 0.25 ppm for CH1000. DP1000 did not absorb diffusible hydrogen from the atmosphere. In terms of the coating's influence, lubrication had a greater impact than coating, resulting in a non-proportional cross-effect when coated material was exposed to water. Similar results were observed for lubricated CH1000 and DH1000, but this did not apply to DP1000.

Declarations

Conflicts of interests

The authors declare no conflict of interest.

References

1. Billur E, Dykeman J, Altan T (2014) Three generations of advanced high-strength steels for automotive applications, Part III: The third generation. Stamping Journal 2014:12–13
2. Hong K-M, Shin YC (2017) Prospects of laser welding technology in the automotive industry: A review. Journal of Materials Processing Technology 245:46–69. https://doi.org/10.1016/j.jmatprotec.2017.02.008
3. Rehrl J (2014) Wasserstoffversprödung in hochfesten, mikrolegierten Stählen. Dissertation, Technische Universität München

4. Gao Q (2017) Investigations on Hydrogen Embrittlement of Advanced High Strength Steels for Automotive Applications. Dissertation, RWTH Aachen University

5. Schaffner T, Hartmaier A, Kokotin V et al. (2018) Analysis of hydrogen diffusion and trapping in ultra-high strength steel grades. Journal of Alloys and Compounds 746:557–566. https://doi.org/10.1016/j.jallcom.2018.02.264

6. Lippold JC (2014) Welding Metallurgy and Weldability, 1., Auflage. John Wiley & Sons, New York, NY

7. Bergmann C (2020) Hydrogen embrittlement resistance evaluation of advanced high strength steel grades in automotive applications, Ruhr-Universität Bochum

8. Schwedler O, Zinke M, Jüttner S (2014) Determination of hydrogen input in welded joints of press-hardened 22MnB5 steel. Weld World 58:339–346. https://doi.org/10.1007/s40194-014-0119-x

9. Schaupp T (2019) Ermittlung geeigneter Wärmeführungen zur Vermeidung wasserstoffunterstützter Kaltrisse beim Schweißen höherfester Feinkornbaustähle mit modifiziertem Sprühlichtbogen : Schlussbericht : Berichtszeitraum: 01.01.2015 bis 30.06.2017. Otto von Guericke University Library, Magdeburg, Germany

10. Schwedler O Wasserstoffunterstützte Kaltrissbildung an Schweißverbindungen von pressgehärtetem 22MnB5. Dissertation, Fakultät für Maschinenbau; Shaker Verlag

11. Loidl M (2014) Entwicklung einer Prüfmethodik zur Charakterisierung höchstfester Karosseriestähle hinsichtlich des Risikos zur Wasserstoff induzierten Rissbildung. Dissertation, Universität Stuttgart

12. Kaesche H (1979) Die Korrosion der Metalle: Physikalisch-chemische Prinzipien und aktuelle Probleme, 2., völlig neubearb. und erw. Aufl. Springer, Berlin, Heidelberg

13. Bailey N, Coe FR, Gooch TG et al. (1973) Welding steels without hydrogen cracking, 2. ed. Abington Publ, Cambridge

14. Pitrun M, Nolan D, Dunne D (2004) Diffusible Hydrogen Content in Rutile Flux-Cored Arc Welds as a Function of the Welding Parameters. Weld World 48:2–13. https://doi.org/10.1007/BF03266408

15. Schwedler O, Holtschke N, Jüttner S (2016) Hydrogen-assisted cold cracking in welded joints of press-hardened 22MnB5. Weld World 60:1063–1070. https://doi.org/10.1007/s40194-016-0364-2

16. Kühn S (2011) Einfluss von diffusiblem Wasserstoff auf die mechanischen Eigenschaften von hochfesten Mehrphasenstählen unter Berücksichtigung der Kaltverfestigung, 1. Aufl. Berichte aus der Werkstofftechnik. Shaker, Aachen

17. Loidl M, Kolk O, Veith S et al. (2011) Characterization of hydrogen embrittlement in automotive advanced high strength steels. Mat.-wiss u Werkstofftech 42:1105–1110. https://doi.org/10.1002/mawe.201100917

18. Drexler A, Bergmann C, Manke G et al. (2021) Local hydrogen accumulation after cold forming and heat treatment in punched advanced high strength steel sheets. Journal of Alloys and Compounds 856:158226. https://doi.org/10.1016/j.jallcom.2020.158226

19. Ogura S, Fukutani K (2018) Thermal Desorption Spectroscopy. In: Japa TSSSo (ed) Compendium of Surface and Interface Analysis. Springer Singapore, Singapore, pp 719–724

20. DIN Deutsches Institut für Normung e.V. DIN EN ISO 3690:2018-12, Schweißen und verwandte Prozesse - Bestimmung des Wasserstoffgehaltes im Lichtbogenschweißgut (ISO 3690:2018); Deutsche Fassung EN ISO 3690:2018

21. American Welding Society Standard methods for determination of the diffusible hydrogen content of martensitic, bainitic, and ferritic steel weld metal produced by arc welding(AWS A4.3-93)

22. JIS – Japanese Standard Association (1975) JIS Z 3113:1975: Method for Measurement of Hydrogen Evolved from Deposited Metal

23. Kuhlmann M, Schwedler O, Holtschke N et al. (2015) Consideration of hydrogen transport in press-hardened 22MnB5. Materials Testing 57:977–984. https://doi.org/10.3139/120.110808

24. Kuhlmann M (2023) Methode zur Bewertung der wasserstoffunterstützten und flüssigmetallinduzierten Versprödung von Fügeelementen aus höchstfesten borlegierten Vergütungsstählen im Ersatzversuch. Dissertation, Fakultät für Maschinenbau; Shaker Verlag

25. Cho S, Kim G-I, Ko S-J et al. (2022) Comparison of Hydrogen Embrittlement Susceptibility of Different Types of Advanced High-Strength Steels. Materials (Basel) 15. https://doi.org/10.3390/ma15093406

26. Rhode M, Schaupp T, Muenster C et al. (2019) Hydrogen determination in welded specimens by carrier gas hot extraction—a review on the main parameters and their effects on hydrogen measurement. Weld World 63:511–526. https://doi.org/10.1007/s40194-018-0664-9

27. Backhaus F (2022) Einflussgrößen auf die Wasserstoffaufnahme und Wasserstoffeffusion hochfester Stähle. Dissertation, Ruhr-Universität Bochum

28. Ilschner B, Heumann T, Mehrer H (1992) Diffusion in Metallen, vol 10. Springer Berlin Heidelberg, Berlin, Heidelberg

29. Choo WY, Lee JY (1982) Thermal analysis of trapped hydrogen in pure iron. Metall and Mat Trans A 13:135–140. https://doi.org/10.1007/BF02642424

30. Hopf A, Klug M, Durmaz K et al. (2023) Introduction of a New Test Methodology for Determining the Delayed Cracking Susceptibility. JMMP 7:26. https://doi.org/10.3390/jmmp7010026

31. Maroef I, Olson DL, Eberhart M et al. (2002) Hydrogen trapping in ferritic steel weld metal. International Materials Reviews 47:191–223. https://doi.org/10.1179/095066002225006548

32. Nagumo M (2016) Fundamentals of Hydrogen Embrittlement. Springer Singapore, Singapore

33. Kannengiesser T, Lausch T (2012) Diffusible Hydrogen Content Depending on Welding and Cooling Parameters. Weld World 56:26–33. https://doi.org/10.1007/BF03321392

34. Padhy GK, Komizo Y (eds) (2013) Diffusible Hydrogen in Steel Weldments: A Status Review. Transactions of Joining and Welding Research Institute(42)

35. Klett J, Wolf T, Maier HJ et al. (2020) The Applicability of the Standard DIN EN ISO 3690 for the Analysis of Diffusible Hydrogen Content in Underwater Wet Welding. Materials (Basel) 13. https://doi.org/10.3390/ma13173750

36. Yurioka N, Suzuki H (1990) Hydrogen assisted cracking in C-Mn and low alloy steel weldments. International Materials Reviews 35:217–249. https://doi.org/10.1179/095066090790323957

37. Stahlinstitut VDEh (2011) SEP 1220-3:2011-08 - Prüf- und Dokumentationsrichtlinie für die Fügeeignung von Feinblechen aus Stahl - Teil 3: Laserstrahlschweißen

38. Maeda K, Suzuki R, Suga T et al. (2020) Investigating delayed cracking behaviour in laser welds of high strength steel sheets using an X-ray transmission in-situ observation system. Science and Technology of Welding and Joining 25:377–382. https://doi.org/10.1080/13621718.2020.1714873

39. Li Y, Zhang K, Lu D et al. (2021) Hydrogen-Assisted Brittle Fracture Behavior of Low Alloy 30CrMo Steel Based on the Combination of Experimental and Numerical Analyses. Materials (Basel) 14. https://doi.org/10.3390/ma14133711

40. Möser M (1980) Zur Wasserstofffrissigkeit nach dem Schweißen, vol 64, Düsseldorf

41. Molodov K (2022) Microstructure evolution in a hot-dip galvanized complex phase gigapascal steel "CH1000". 6th International Conference on Steels in Cars and Trucks, Mailand

42. Chen X, Niu C, Lian C et al. (2017) The Evaluation of Formability of the 3rd Generation Advanced High Strength Steels QP980 based on Digital Image Correlation Method. Procedia Engineering 207:556–561. https://doi.org/10.1016/j.proeng.2017.10.1020

43. Park C, Kang N, Liu S (2017) Effect of grain size on the resistance to hydrogen embrittlement of API 2W Grade 60 steels using in situ slow-strain-rate testing. Corrosion Science 128:33–41. https://doi.org/10.1016/j.corsci.2017.08.032

44. Yazdipour N, Dunne DP, Pereloma EV (2012) Effect of Grain Size on the Hydrogen Diffusion Process in Steel Using Cellular Automaton Approach. MSF 706-709:1568–1573. https://doi.org/10.4028/www.scientific.net/MSF.706-709.1568

45. Kuron D (ed) (1986) Wasserstoff und Korrosion: Festschrift zum 60. Geburtstag von Hubert Gräfen. Bonner Studienreihe, vol 3. Kuron, Bonn

46. Pohl M (2014) Hydrogen in Metals: A Systematic Overview. Practical Metallography 51:291–305. https://doi.org/10.3139/147.110295

47. Okuda N, Ogata Y, Nishikawa Y. et al. (1987) Hydrogen-Induced Cracking Susceptibility in High-Strength Weld Metal: A formula is proposed to estimate minimum preheat and interpass temperatures which help prevent hydrogen-induced cracking. Welding Research Supplement:S. 141-146

48. COTTERILL P, KING J (1991) Hydrogen embrittlement contributions to fatigue crack growth in a structural steel. International Journal of Fatigue 13:447–452. https://doi.org/10.1016/0142-1123(91)90478-H

49. Kim H-J, Lee M-G, Yoon S-C et al. (2020) Diffusible hydrogen behavior and delayed fracture of cold rolled martensitic steel in consideration of automotive manufacturing process and vehicle service environment. Journal of Materials Research and Technology 9:13483–13501. https://doi.org/10.1016/j.jmrt.2020.09.113

50. Kim H-J, Lee M-G (2022) Analysis of hydrogen trapping behaviour in plastically deformed quenching and partitioning steel in relation to microstructure evolution by phase transformation. Journal of Alloys and Compounds 904:164018. https://doi.org/10.1016/j.jallcom.2022.164018

51. Koyama M, Springer H, Merzlikin SV et al. (2014) Hydrogen embrittlement associated with strain localization in a precipitation-hardened Fe−Mn−Al−C light weight austenitic steel. International Journal of Hydrogen Energy 39:4634–4646. https://doi.org/10.1016/j.ijhydene.2013.12.171

52. Rhode M (2016) Hydrogen diffusion and effect on degradation in welded microstructures of creep-resistant low-alloyed steels. Bundesanstalt für Materialforschung und -prüfung (BAM), Berlin

53. Zinke M (2019) Untersuchung des Wasserstoffgefährdungspotentials warmumgeformter Bauteile aus hochfestem Stahl : Schlussbericht der Forschungsstelle(n) Otto-von-Guericke-Universität Magdeburg, Institut für Werkstoff- und Fügetechnik (IWF) zu dem über die im Rahmen des Programms zur Förderung der Industriellen Gemeinschaftsforschung und -entwicklung (IGF) … geförderten Vorhaben … ; Bewilligungszeitraum: 01.07.2011 – 30.06.2013. Otto von Guericke University Library, Magdeburg, Germany

54. Beachem CD (1972) A new model for hydrogen-assisted cracking (hydrogen "embrittlement"). MTB 3:441–455. https://doi.org/10.1007/bf02642048

55. Martin ML, Robertson IM, Sofronis P (2011) Interpreting hydrogen-induced fracture surfaces in terms of deformation processes: A new approach. Acta Materialia 59:3680–3687. https://doi.org/10.1016/j.actamat.2011.03.002

56. Robertson IM, Sofronis P, Nagao A et al. (2015) Hydrogen Embrittlement Understood. MTB 46:1085–1103. https://doi.org/10.1007/s11663-015-0325-y

Footnotes

[1] Carbon equivalent according to Yurioka et al. [36]

$$CEQ = C + A(C) \times B(C)$$

$$A(C) = [0.75 + 0.25 \times \tanh(20 \times (C - 0.12))]$$

$$B(C) = [Si/24 + Mn/6 + Cu/15 + Ni/60 + (Cr + Mo + Nb + V)/5 + 5 \times B]$$

Figures
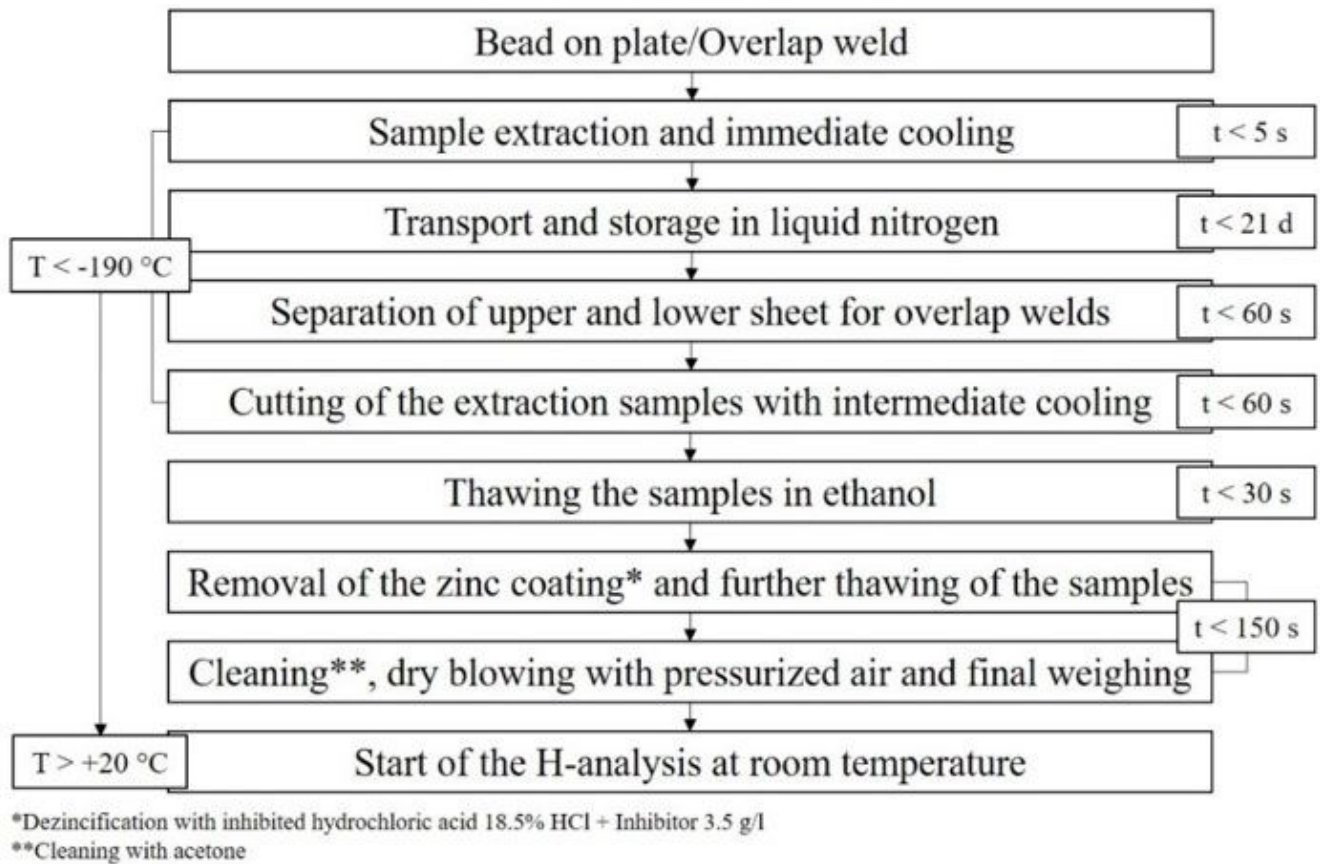
Figure 1

Procedure showing all steps from welding to measurement with corresponding working times and temperature of the samples
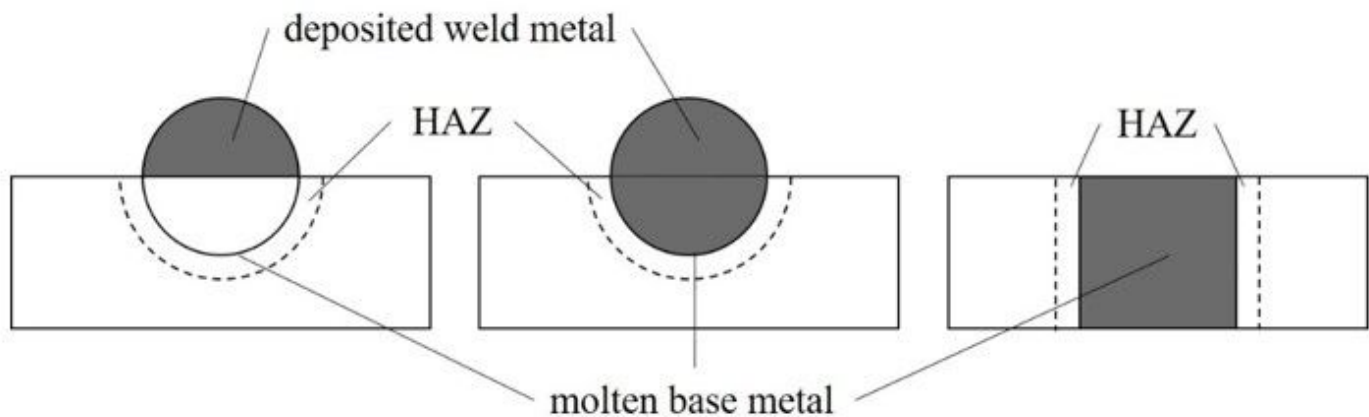

Figure 2

Schematic view of different weld bead micro sections; left: deposited weld metal only (H_D), middle: deposited weld metal and molten base metal (H_F), right: molten base metal only (H_{LW})
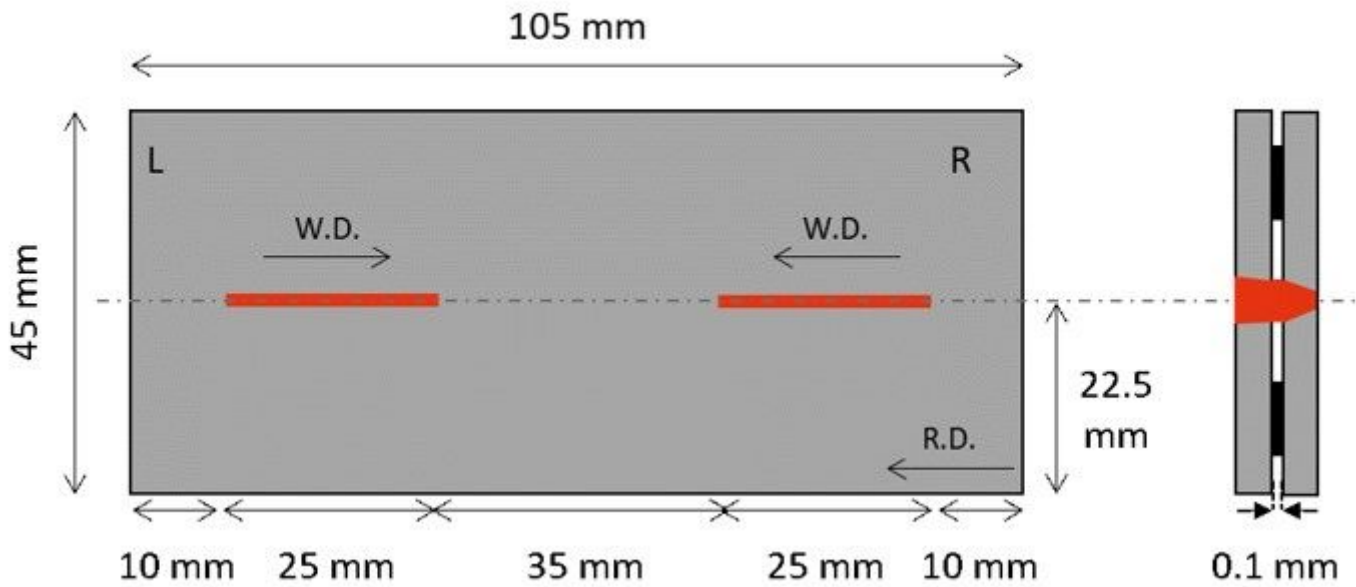
Figure 3

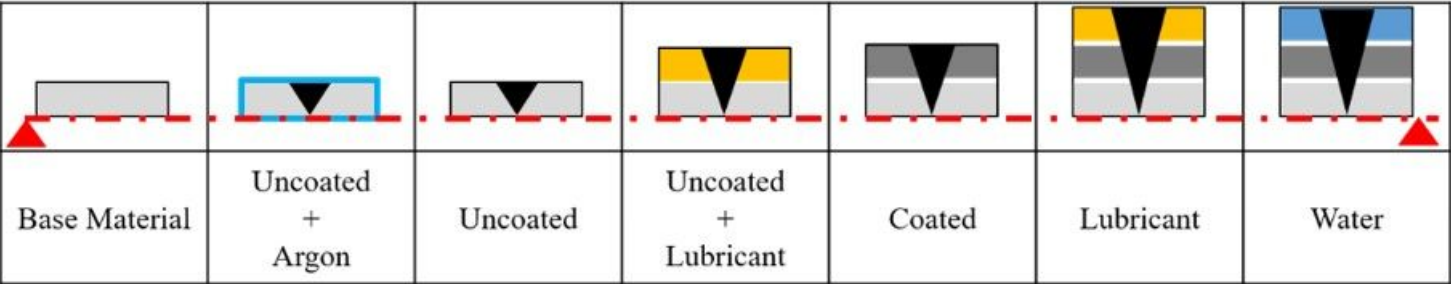Sample geometry of the cold cracking test for laser-welded joints [30]

| Base Material | Uncoated + Argon | Uncoated | Uncoated + Lubricant | Coated | Lubricant | Water |

Figure 4

Schematic overview of different surface conditions with mirror plane (red) for overlapping welding experiments
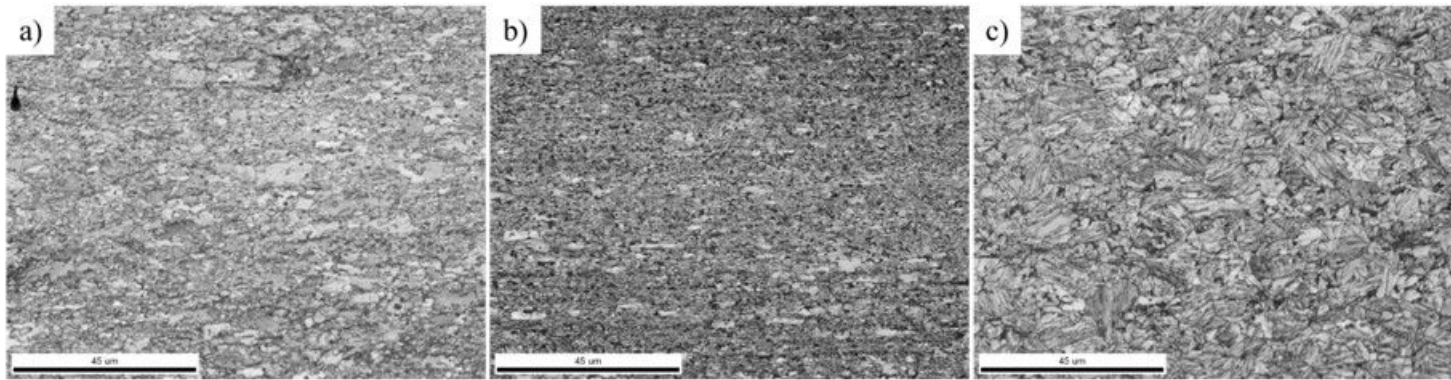
Figure 5

Microstructure of CH1000 a), DP1000 b) and DH1000 c)
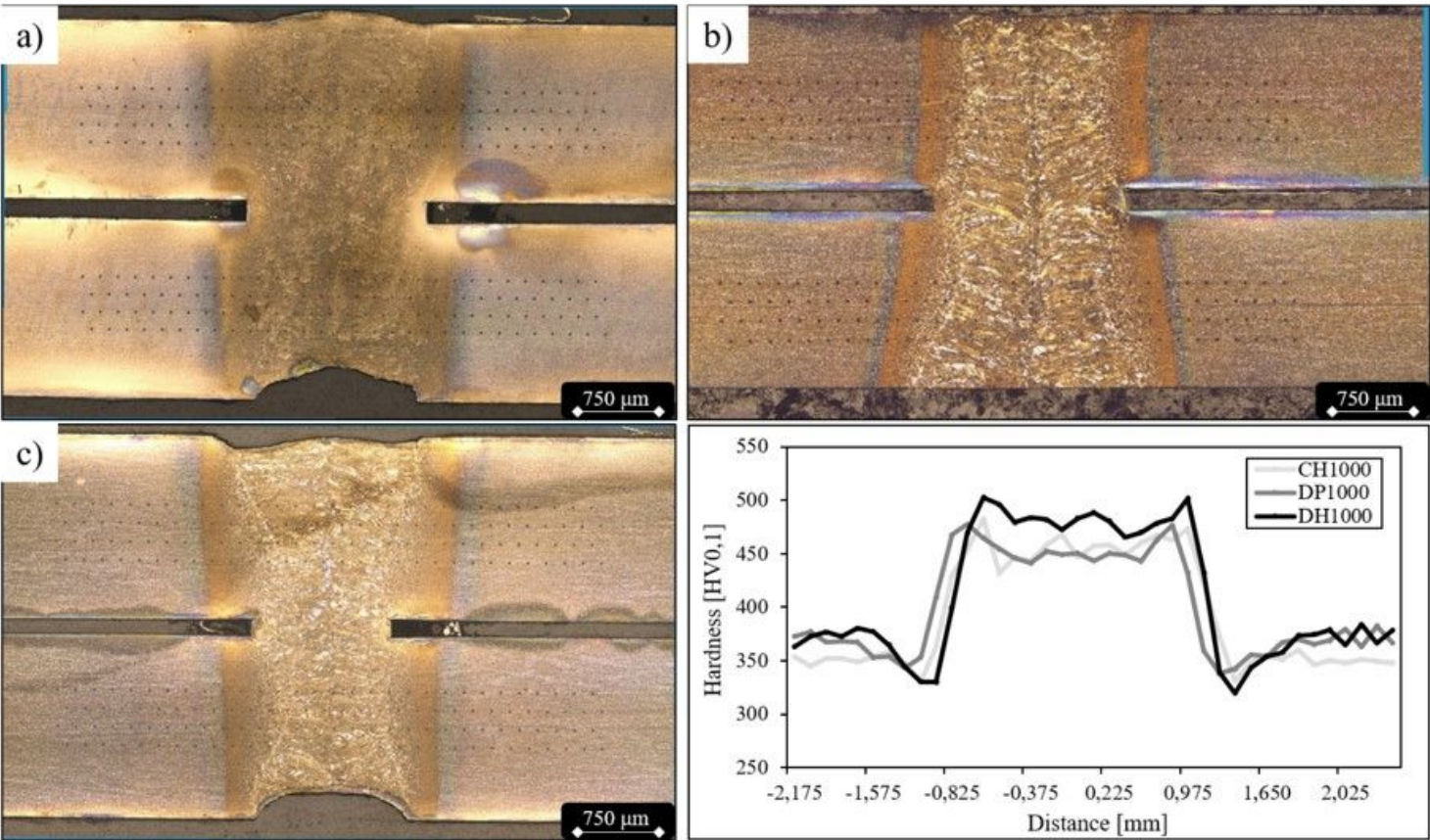
Figure 6

Cross section and hardness profiles of DH1000 a), CH1000 b) and DP1000 c)
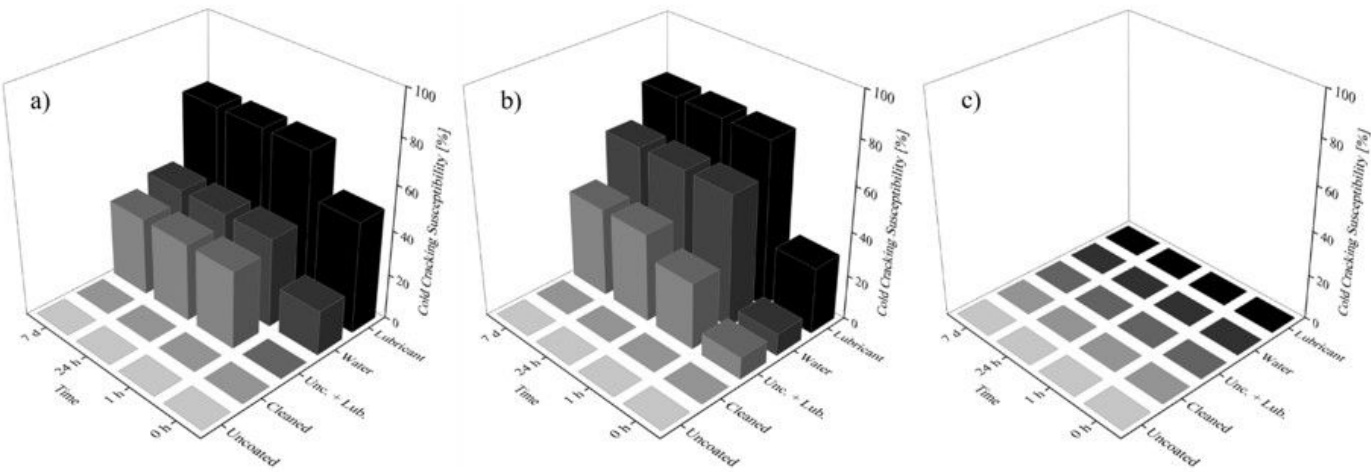
Figure 7

Cold cracking susceptibility of DH1000 a), CH1000 b) and DP1000 c)
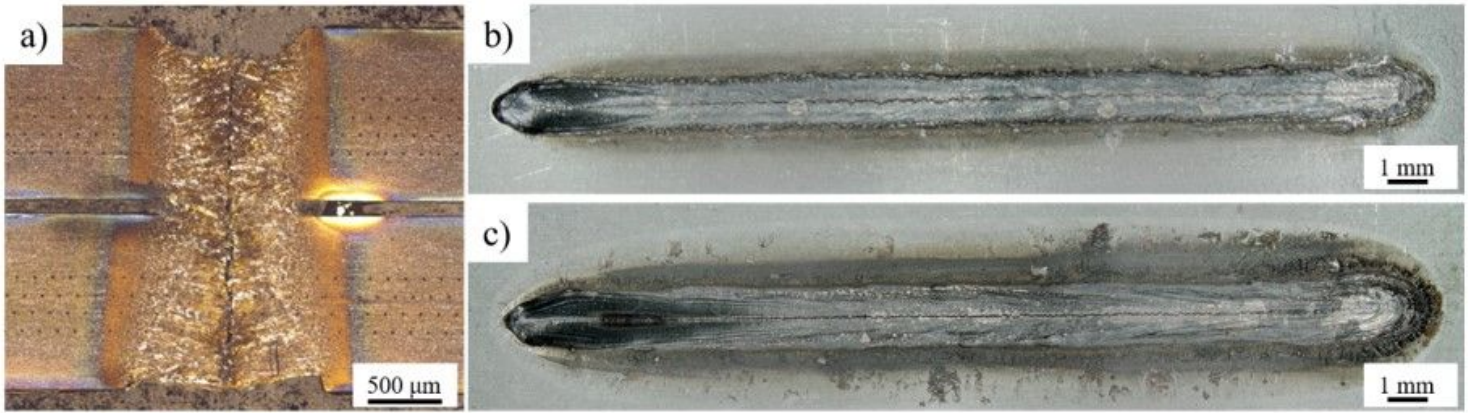
Figure 8

Cross section a) and top b) and bottom c) surface of a cracked CH1000 coated and lubricated weld seam
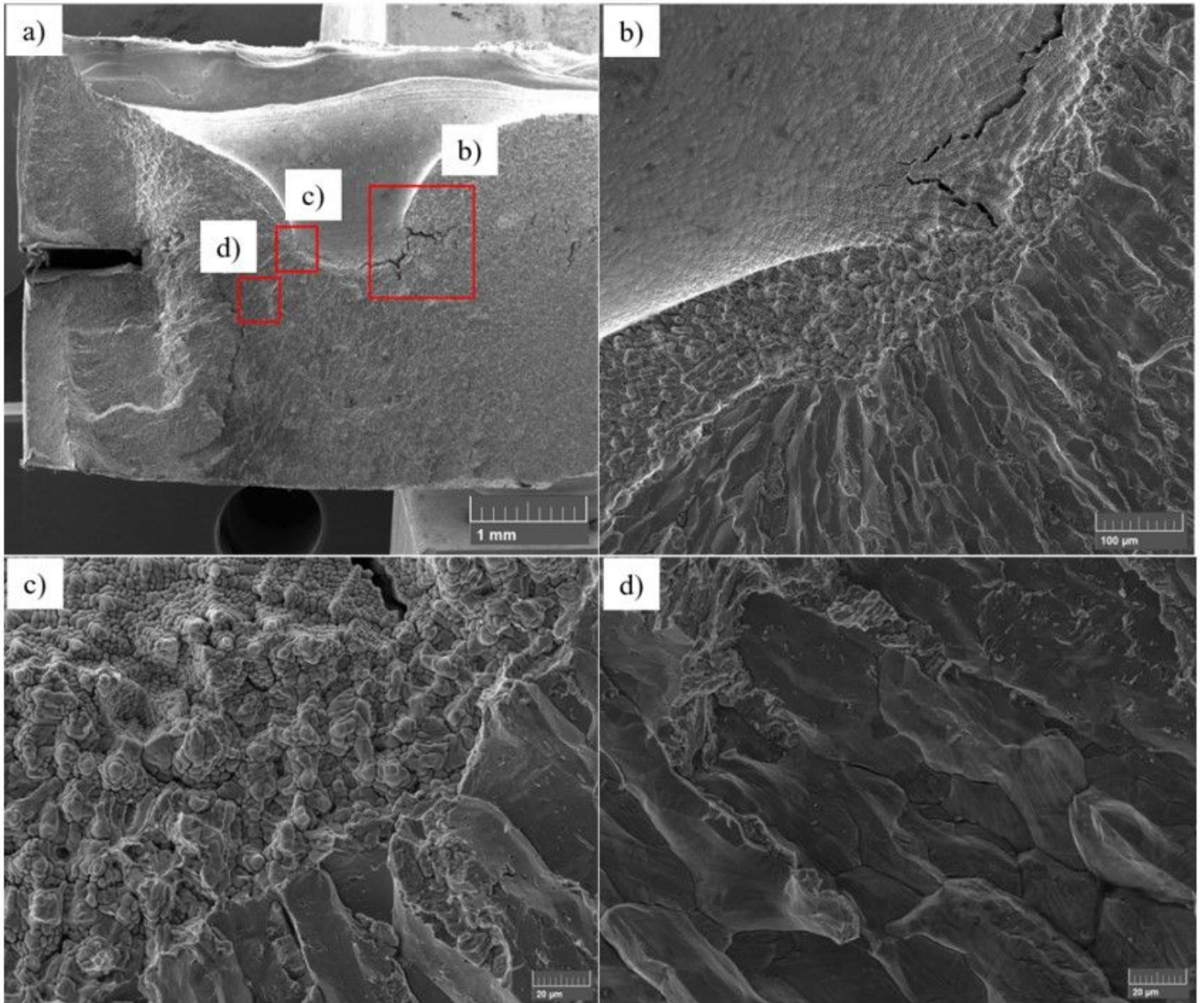
Figure 9

SEM images of the end crater a), mixed crack surfaces of hot and cold crack area b), detailed image of dendritic hot crack area c) and detail of trans- and intergranular fracture in cold crack area d) exemplary for DH1000 coated and lubricated
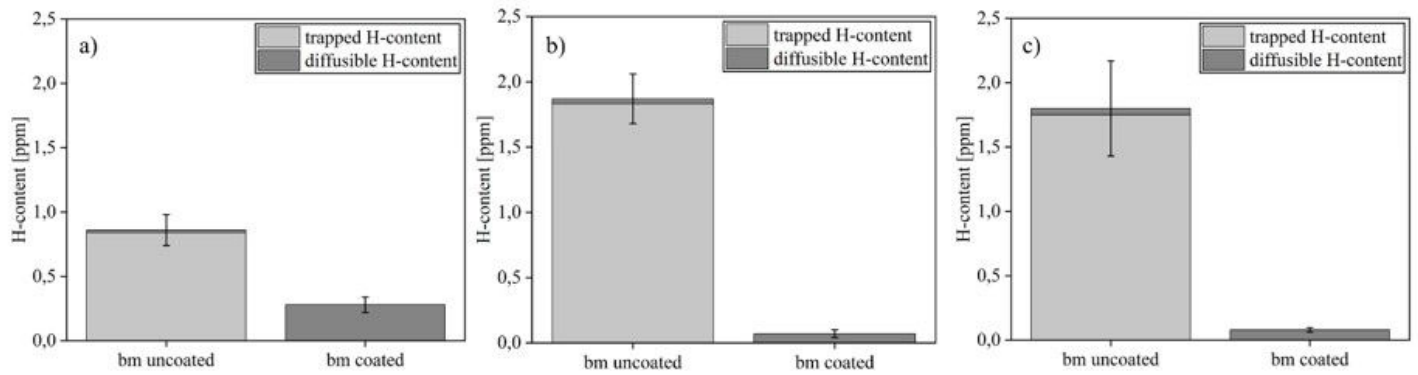
Figure 10

Total hydrogen content of uncoated base material measured with ME at 1800 °C and diffusible hydrogen contents of coated and uncoated material measured with TDS at 300 °C of DH1000 a), CH1000 b) and DP1000 c)
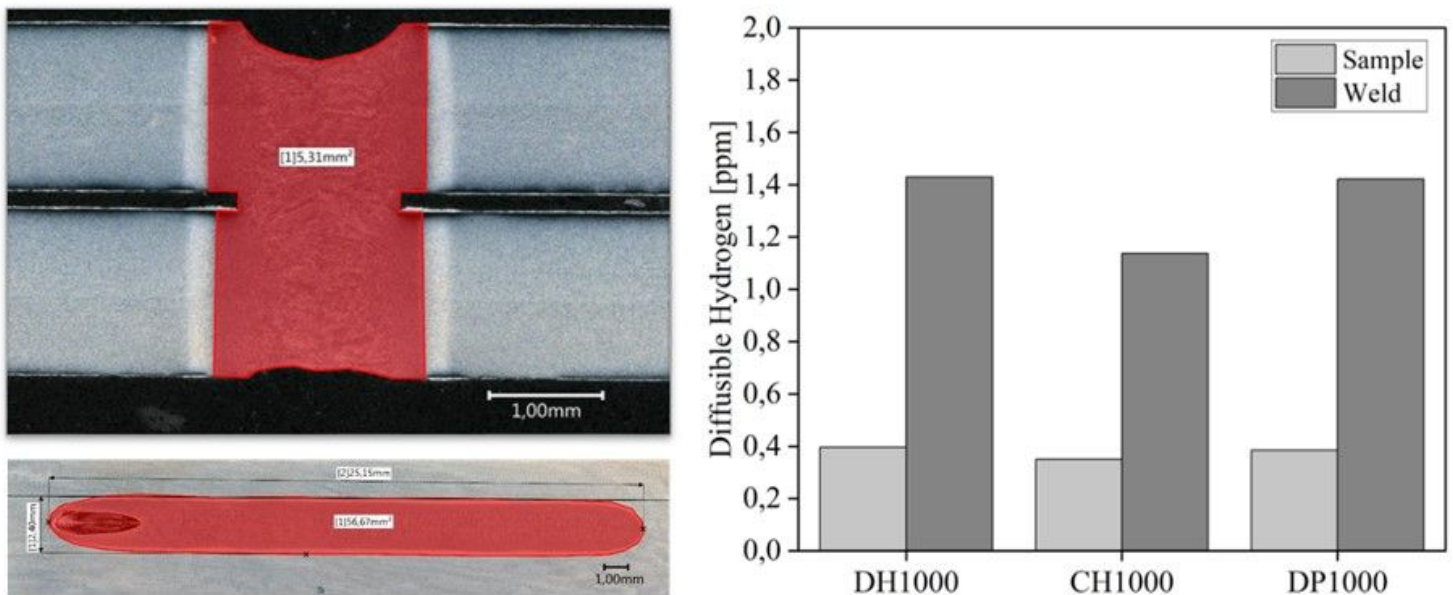

Figure 11

Exemplary Weld pool area in transversal and longitudinal direction for DP1000 and effect of normalizing hydrogen contents from whole sample to the weld, exemplary for coated welds of all materials
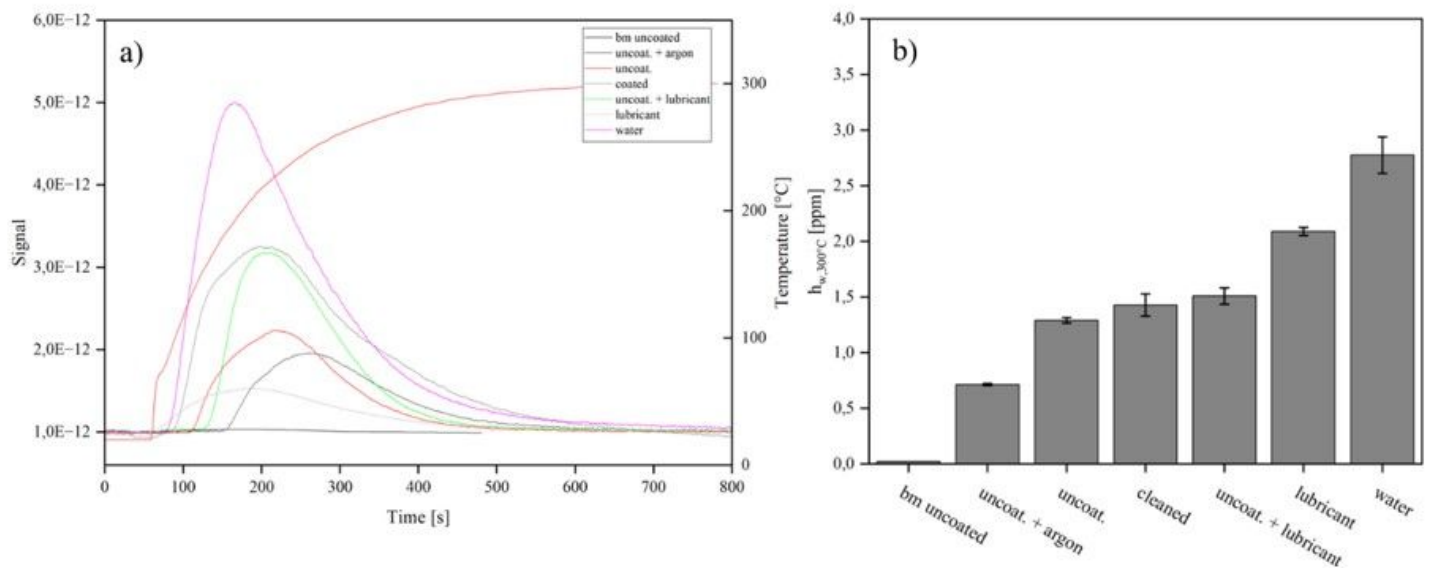
Figure 12

Measured TDS spectra and temperature curve a) and resulting diffusible hydrogen amount b) in the weld seams of DH1000
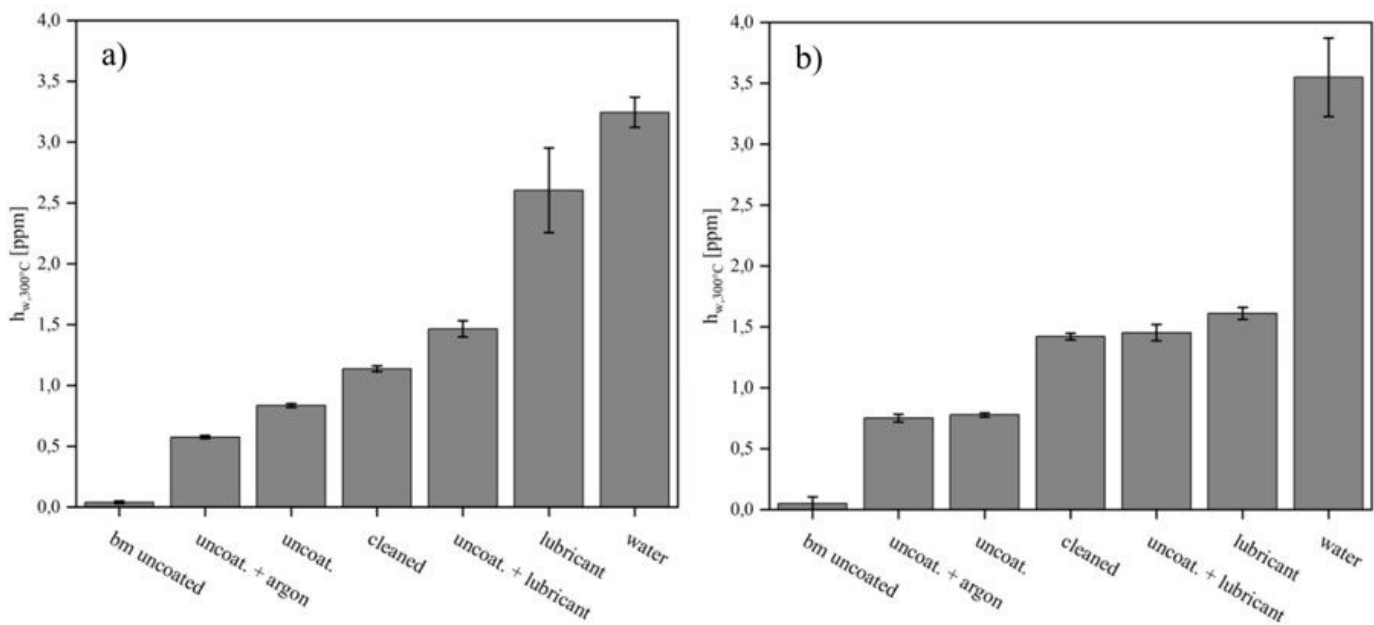

Figure 13

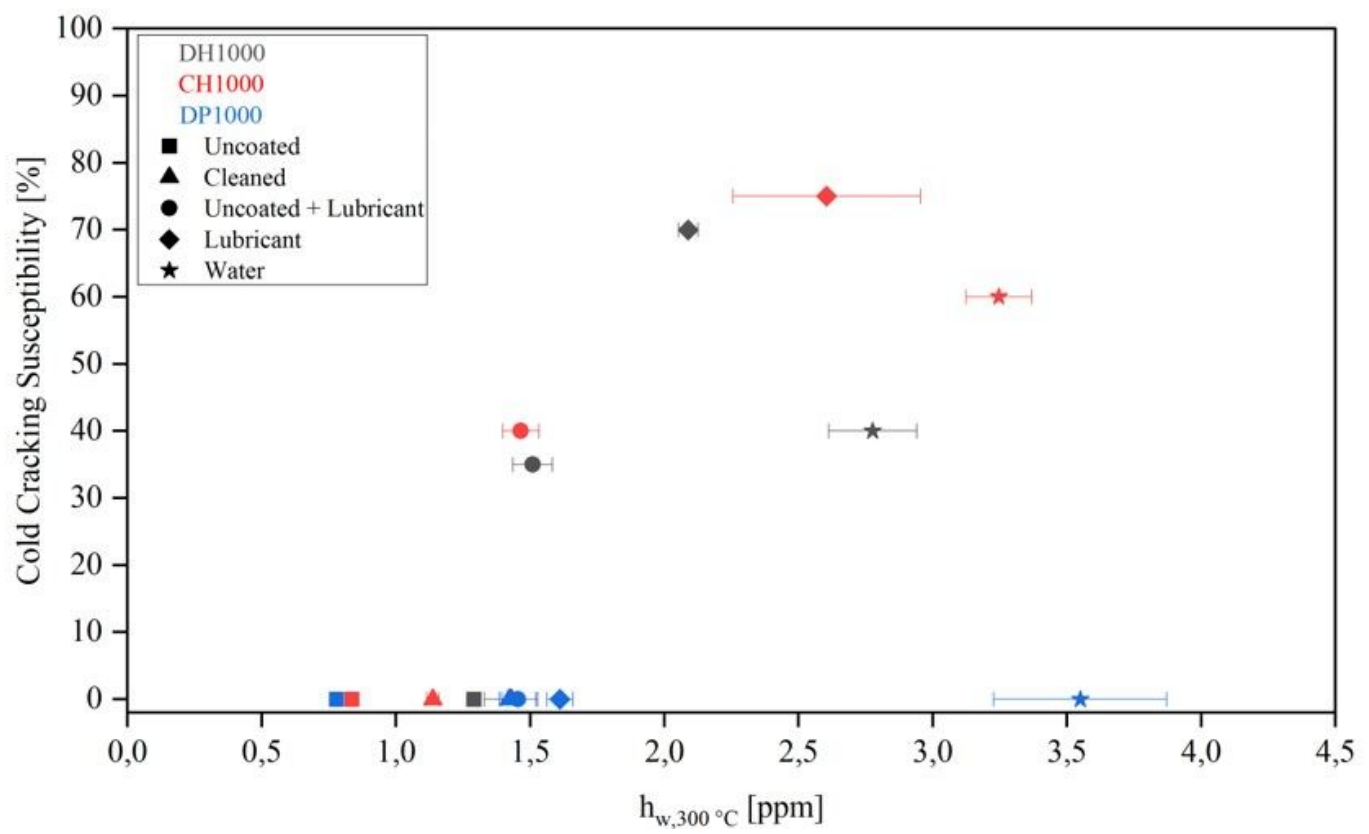Diffusible hydrogen content in the weld of CH1000 a) and DP1000 b)

Figure 14

Correlation of measured diffusible hydrogen contents in welds $h_{w,300°C}$ and cold cracking susceptibility